Aluminum Toxicity Elicits a Dysfunctional TCA Cycle and Succinate Accumulation in Hepatocytes

Ryan J. Mailloux, Robert Hamel, and Vasu D. Appanna

Department of Chemistry and Biochemistry, Laurentian University, Sudbury, Ontario, Canada, P3E 2C6; E-mail: *vappanna@laurentian.ca*

Received 25 April 2006; revised 7 June 2006; accepted 12 June 2006

ABSTRACT: Aluminum (Al), a known environmental toxicant, has been linked to a variety of pathological conditions such as dialysis dementia, osteomalacia, Alzheimer's disease, and Parkinson's disease. However, its precise role in the pathogenesis of these disorders is not fully understood. Using hepatocytes as a model system, we have probed the impact of this trivalent metal on the aerobic energy-generating machinery. Here we show that Al-exposed hepatocytes were characterized by lipid and protein oxidation and a dysfunctional tricarboxylic acid (TCA) cycle. BN-PAGE, SDS-PAGE, and Western blot analyses revealed a marked decrease in activity and expression of succinate dehydrogenase (SDH), α-ketoglutarate dehydrogenase (KGDH), isocitrate dehydrogenase-NAD$^+$ (IDH), fumarase (FUM), aconitase (ACN), and cytochrome *c* oxidase (Cyt C Ox). ^{13}C-NMR and HPLC studies further confirmed the disparate metabolism operative in control and Al-stressed cells and provided evidence for the accumulation of succinate in the latter cultures. In conclusion, these results suggest that Al toxicity promotes a dysfunctional TCA cycle and impedes ATP production, events that may contribute to various Al-induced abnormalities. © 2006 Wiley Periodicals, Inc. J Biochem Mol Toxicol 20:198–208, 2006; Published online in Wiley InterScience (www.interscience.wiley.com). DOI 10:1002/jbt.20137

KEYWORDS: **Aluminum; TCA Cycle; Succinate; ATP**

INTRODUCTION

Aluminum (Al) has become an important health concern due to its increased bioavailability triggered by acid rain and anthropogenic activities. Exposure to this trivalent metal has also been on the rise as it is widely utilized in antacids, the processing of potable water, and various food products [1]. Al does not appear to have any biological function but is notorious for its toxic influence. Iron homeostasis, Ca^{2+}-mediated processes, membrane lipids, and Mg^{2+}-catalyzed reactions appear to be the primary targets of Al [2]. The iron-depleted situation generated by Al has been shown to lead to elevated transferrin receptor synthesis and the suppression of ferritin production [2,3]. Furthermore, the oxidative environment promoted by Al toxicity has been shown to result in the alteration of membrane fluidity, hence, abnormal biological functions [4].

Pathological conditions such as Alzheimer's disease, Parkinson's disease, amyotrophic lateral sclerosis, and Down's syndrome have all been associated with increased accumulation of Al in cerebral tissues [3]. Following absorption of Al via the gastrointestinal system, the metal gains entry to the liver, kidney, lungs, and spleen with the assistance of the transferrin uptake machinery or the involvement of organic chelators such as citrate, malate, lactate, or succinate [3]. In the transferrin-mediated uptake system, Al competes with Fe and gains access to the cell with the aid of the receptor-mediated endocytosis [5]. Once inside the cell, Al exerts its toxic properties by substituting for iron in Fe-dependent proteins, thus preventing redox reactions [6]. Although the impact of Al on Fe-mediated reactions has been reported [7], the influence of this metal on metabolic processes has not been fully delineated. The tricarboxylic acid (TCA) cycle is a key metabolic pathway that provides the cell with energy and anabolic precursors for proliferation and survival [8]. As these processes are mediated by metal cofactors and essential sulfur groups localized in various enzymes, it is important to elucidate how Al toxicity interferes with these critical energy-generating systems.

In this study, HepG2 cells were used as a model system to elucidate the effects of Al on key metabolic enzymes that are involved in energy production. Here we report on the ability of Al to create an oxidative environment and to impede the TCA cycle by interfering

Correspondence to: Vasu D. Appanna.

Contract Grant Sponsor: Industry Canada and Human Resources and Development Canada.

with the expression and activity of such enzymes as succinate dehydrogenase (SDH) and aconitase (ACN). This metabolic dysfunction appears to promote the accumulation of succinate. The implication of these findings on cellular energy status and the role of succinate as a signaling molecule are also discussed.

MATERIALS AND METHODS

Cell Culture and Isolation

HepG2 cells were a gift from Dr. D. Templeton (University of Toronto) and were maintained in α-MEM supplemented with 5% FBS and 1% antibiotics. Cells were routinely seeded and cultured in 175 cm^2 flasks with loosened caps and incubated with 5% CO_2 in a humidified atmosphere at 37°C.

Al Treatment and Cell Viability

Upon reaching 70% confluency, the cell cultures were re-supplemented with serum-free media containing citrate (2.5 mM) or Al–citrate (0.5 mM:2.5 mM) and exposed from 4 to 24 h. (*Note*: The amount of Al utilized ranged from 0.2 to 13.4 μg/mL compared to 750 μg/mL in Alzheimer's serum, >0.4 μg/mL in serum from dialysis patients, and the allowable limit of 0.1–10 μg/mL in drinking water [3,9–13].) Recovery assays were performed on Al-stressed cells transferred in the FBS medium for 24 h. Cell viability was monitored with the aid of the Trypan Blue Exclusion Assay [14]. The concentration of citrate utilized is similar to the amount found in human serum. At the desired time intervals, cells were trypsinized and centrifuged at 450*g* for 10 min at 4°C. Following two washings with PBS, the pellet was suspended in cell storage buffer (CSB) (50 mM Tris–HCl, 1 mM phenylmethylsulfonylfluoride, 1 mM dithiothreitol, 250 mM sucrose, 2 mM citrate) and stored at −86°C until needed.

Aluminum Measurement and Visualization

Analysis of Al metabolism in HepG2 cells was done using the Aluminon Assay [15]. Following washings with 0.1 mM EDTA and PBS (to remove any fortuitously bound Al), 4×10^6 cells were ultrasonically disrupted (20 s in 2 s bursts with a Brunswick sonicator). The membrane and soluble fractions were isolated by centrifugation at 180,000*g* for 3 h at 4°C. While the soluble fraction and the spent fluid were analyzed without further treatment, the membrane fraction was treated with conc. nitric acid at 95°C for 4 h to hydrolyze all membrane bound protein. The absorbance was measured at 530 nm. $AlCl_3$ was used as the standard.

Morin reagent was used to visualize the relative amount of Al associated in HepG2 cells. Following the exposure of the cells to citrate or Al–citrate, cells were washed twice with PBS and once with 0.5 mM EDTA. Hepatocytes were fixed with methanol:glacial acetic acid (3:1) and exposed to rhodamine B (10 μg/mL in 2 mL of MEM + 5% FBS) for 30 min at 37°C. This allowed the optical detection of the mitochondria [16]. This was followed by counterstaining with 0.1 mg/mL of morin reagent for 10 min [17]. The coverslips were washed thoroughly with PBS and mounted for detection. The cells were then visualized using an inverted deconvoluting microscope (Zeiss). The Al–morin complex was detected at $\lambda_{excitation} = 425$ nm and $\lambda_{emission} = 520$ nm and protonated rhodamine B was ascertained at $\lambda_{excitation} = 546$ nm and $\lambda_{emission} = 620$ nm. In vitro binding assays were performed to optimize the assay, to ensure Al specificity, and to prevent spectral overlap of the two fluorophores.

Oxidized Protein and Lipid Analysis

The Thiobarbituric Acid Reactive Species Assay (TBARS) was performed in order to evaluate the amount of oxidized lipids in the membrane, according to the method in [18]. The membrane fraction was solubilized in a mixture of 15% trichloroacetic acid, 0.375% trichlorobarbituric acid, and 0.25 N HCl. The reaction mixture was heated for 25 min at 95°C. The precipitated protein was spun down at 21,000*g* for 10 min and the clear supernatant was measured at 532 nm.

Determination of protein carbonyl content was performed with the dinitrophenyl hydrazine (DNPH) assay [19]. One milligram of soluble protein was mixed with 1 mL of 2% (w/v) DNPH and allowed to stand for 1 h. Following precipitation of the protein, the pellet was washed three times with ethylacetate:ethanol (1:1). The resultant mixture, obtained after the addition of 1 mL of 6 M guanidine–HCl, was read at 360 nm.

Subcellular Fractionation

The cells were thawed and pelleted at 450*g* for 10 min at 4°C and resuspended in CSB containing 1 mg/mL of pepstatin A and 0.1 mg/mL of leupeptin. The cell suspension was homogenized on ice using a Brunswick sonicator for 20 s in 2 s bursts. Following homogenization, mitochondrial and soluble fractions were isolated by differential centrifugation [20,21]. The nucleus and whole cells were removed by centrifugation at 700*g* for 10 min at 4°C. The supernatant was then subjected to centrifugation at 12,000*g* for 30 min at 4°C to pellet the mitochondria. The mitochondrial pellet was then resuspended in a minimal amount of

CSB. The supernatant was utilized to monitor the soluble enzymes. The purity of the cellular fractions were confirmed by immunoblot analysis of F-actin, voltage-dependent anion channel (VDAC), and histone 2A.

In Vitro Identification of Fe–S Cluster Stability

Fe–S cluster stability was determined by scanning 0.5 mg/mL of protein equivalent of mitochondria from control or Al-stressed cultures. The state of the Fe–S cluster was ascertained by performing a UV–VIS scan using an Ultraspec 2100 Pro spectrophotometer. The Fe–S cluster attributed to 395–420 nm was monitored [22,23].

^{13}C-Nuclear Magnetic Resonance Studies

^{13}C-NMR analyses were performed using a Varian Gemini 2000 spectrometer operating at 50.38 MHz for ^{13}C. Experiments were executed with a 5 mm dual probe (35° pulse, 1-s relaxation delay, 8 kilobytes of data, and 2000 scans). Chemical shifts were referenced to standard compounds under the same conditions. Following exposure to Al, whole cells were exposed to 10 mM [2,4-^{13}C] citrate for 1 h at 37°C. Similar experiments were performed with control cells. Mitochondria were isolated from control and Al-exposed HepG2 cells and 1 mg of protein, equivalent of mitochondria, was incubated at 37°C with 5 mM [2,3-^{13}C] succinate + 1 mM NAD^+. The reaction was performed in a 1.5 mL microfuge tube for 1 h and was stopped by placing the tube in boiling H_2O for 5 min. Following the removal of any precipitate, the ^{13}C-NMR spectra were recorded.

Blue Native-PAGE and Two-Dimensional Electrophoretic Analysis

Blue Native (BN)-PAGE was performed according to the method of Schagger [24,25]. The BioRad MiniProtean™ 2 system was utilized, and 4–10% linear gradient gels were favored for protein separation. Mitochondrial proteins were prepared in BN buffer (500 mM 6-amino hexanoic acid, 50 mM BisTris (pH 7.0), and 1% β-dodecyl-D-maltoside). The soluble protein was prepared in a similar manner except maltoside was omitted. Thirty micrograms of protein/lane was loaded in each well. Gels were electrophoresed under native conditions. Eighty volt was used for the stacking gel and increased to 200 V upon entering the resolving gel. The blue cathode buffer (50 mM Tricine, 15 mM BisTris, 0.02% Coomassie G-250 (pH 7.0) at 4°C) was changed to colorless cathode buffer (50 mM Tricine, 15 mM BisTris, (pH 7.0) at 4°C) when the running front was half way through the separating gel. Electrophoresis was stopped just as the running front reached the bottom of the gel. The gel was then placed in equilibration buffer (25 mM Tris, 5 mM $MgCl_2$ (pH 7.4) for 15 min). Enzyme activity was visualized by formazan formation in a reaction buffer consisting of equilibration buffer, 5 mM substrate, 0.5 mM cofactor, 0.5 mg/mL iodonitrotetrazolium, and 0.2 mg/mL phenazine methosulfate [8]. Isocitrate dehydrogenase (IDH) activity staining was performed with the aid of isocitrate (5 mM), NAD^+ (0.1 mM), phenazine methosulfate, and iodonitrotetrazolium. Malate dehydrogenase (MDH) and α-ketoglutarate dehydrogenase (KGDH) were detected using the same technique except malate (5 mM) and α-ketoglutarate (αKG) (5 mM) were the substrates and 0.25 mM CoA was an additional cofactor. SDH activity was visualized using succinate (60 mM), 5 mM KCN, phenazine methosulfate, and iodonitrotetrazolium. ACN activity was detected in a reaction buffer consisting of 5 mM citrate, 0.5 mM $NADP^+$, 5 units/mL IDH-$NADP^+$ (Sigma), iodonitrotetrazolium, and phenazine methosulfate. Similarly, for fumarase (FUM), fumarate (5 mM), NAD^+ (0.5 mM), iodonitrotetrazolium, phenazine methosulfate, and MDH (5 units/mL) were utilized [4]. Cytochrome *c* oxidase (Cyt C Ox) activity was tested with equilibration buffer supplemented with 5 mM KCN, diaminobenzidene (10 mg/mL), cytochrome *c* (10 mg/mL), and sucrose (562.5 mg/mL) [26]. Two-dimensional BN-PAGE and SDS-PAGE were performed on the activity bands. Protein content was examined by Coomassie Blue stain or silver staining (Biorad). Band specificity was confirmed by loading pure enzyme or performing the reactions in the absence of substrate.

SDS-PAGE and Immunoblots

SDS-PAGE in a discontinuous buffer system was performed according to the modified method of Laemmli [27]. Samples were solubilized in 62.5 mM Tris–HCl (pH 6.8), 2% SDS, and 2% β-mercaptoethanol at 100°C for 5 min. The proteins were transferred to a Hybond™-P polyvinylidene difluoride membrane for immunoblotting. Nonspecific binding sites were blocked by incubating the membrane in 5% nonfat skim milk in TTBS (20 mM Tris–HCl, 0.8% NaCl, 1% Tween-20 (pH 7.6)) for 1 h. Polyclonal antibodies raised against KGDH, SDH, and ACN from rabbits were generously supplied by Dr. G. Lindsay, University of Glasgow; Dr. Lemire, University of Alberta; and Dr. R. Eisenstein, University of Wisconsin–Madison, respectively. VDAC (Abcam) and F-actin (Santa Cruz)

were used as loading controls. The secondary antibody consisted of horseradish peroxidase-conjugated mouse anti-rabbit (Santa Cruz). Detection of the desired antigen was done by incubating the membrane for 5 min at room temperature in Chemiglow (Alpha Innotech). The immunoblots were subsequently documented using the ChemiDoc XRS system (Biorad Imaging Systems). Band intensity was quantified using Alpha Innotech Software (Alpha Innotech Corporation).

Analysis of TCA Cycle Metabolites

To further confirm the disparate metabolism operative in Al-stressed cells, the metabolites were analyzed by HPLC. The spent fluid obtained from these two cultures after 24 h of incubation was analyzed on a C_{18}-reverse phase column (Phenomenex) using an Alliance HPLC purchased from Waters. The mobile phase consisted of 20 mM KH_2PO_4 (pH 2.9 with 6 N HCl) and the column was eluted at a flow rate of 0.7 mL/min at 30°C ambient temperature. The retention time of the organic acids were compared to known standards. The presence of succinate was further ascertained by enzymatic reaction involving SDH obtained from cell-free extract of *Pseudomonas fluorescens*. Dichloroindophenol (DCPIP) was the chromophore [28]. Briefly, spent fluid was lyophilized and reconstituted in ddH_2O and analyzed with 25 μg/mL DCPIP and 0.2 mg/mL protein equivalent/mL of membrane from *P. fluorescens* in a reaction buffer (25 mM Tris–HCl, pH 7.4, 5 mM $MgCl_2$, 5 mM KCN). The decrease in intensity at 600 nm was monitored on an Ultraspec 2100 Pro spectrophotometer.

Mitochondria (2 mg protein equivalent) obtained from control and Al-exposed cells were incubated with 10 mM αKG, 0.1 mM NAD^+, and 0.1 mM CoA at 37°C for 10 min. The reaction was subsequently stopped by boiling and the organic acids were extracted with 0.1% perchlorate. The consumption of αKG was recorded by HPLC as described previously.

RESULTS

Al and Cellular Toxicity

Following the exposure of the cells to citrate and Al–citrate respectively, the distribution of Al in the hepatocytes was examined. Al did appear to interact directly with the cell as nearly 42% of the Al was associated with cells even following washings with 0.1 mM EDTA (Table 1). Bright field microscopy revealed significant morphological changes in HepG2 cells exposed to Al compared to the control cells. The former appeared to be enlarged (Figure 1). These observations were further confirmed when intracellular Al was visualized with the aid of morin reagent. Green fluorescence characteristic of Al was readily evident in the HepG2 cells subjected to Al–citrate treatment, while such fluorescence was absent in hepatocytes incubated with citrate (Figure 1). Counterstaining the cells with rhodamine B, a mitochondrial detector, correlated the green fluorescence of the Al–morin complex with the position of the mitochondria (Figure 1).

TABLE 1. Aluminum Distribution, Oxidized Lipids, and Oxidized Proteins in HepG2 Cells Exposed to Citrate or Al–Citrate for a 24 h Period

Treatment	*Amount of Al in Cells ($\mu g/4 \times 10^6$ Cells)*	*Oxidized Lipids ($\mu mol^a/4 \times 10^6$ Cells)*	*Oxidized Protein ($pmol^b/4 \times 10^6$ Cells)*
Control	0.513 ± (0.663)	0.024 ± (0.001)	0.465 ± (0.002)
Al-stressed	56.245 ± (1.194)	0.609 ± (0.017)	1.302 ± (0.007)

$n = 3$, mean ± SD in parentheses.
[a] Malondialdehyde equivalents (μmol).
[b] Carbonyl equivalents (pmol).

Al as a Promoter of Oxidative Stress

As Al toxicity has been shown to be mediated by an oxidative environment, the amount of oxidized lipids and proteins in control and Al-treated HepG2 cells was analyzed. Table 1 depicts the amount of carbonyl residue associated with the soluble CFE obtained from control and Al-stressed HepG2 cells. After 24 h, a three-fold increase was attained in the Al-stressed cells. Similarly, oxidized lipids, as monitored by TBARS assay, increased sharply in cells subjected to Al–citrate for 24 h (Table 1). These findings prompted us to examine how the cellular metabolism might be affected by the presence of Al in the medium.

Proton-Decoupled ^{13}C-NMR and HPLC Studies

HepG2 cells isolated from Al-stressed and control cultures were incubated with [2,4-^{13}C] citrate for 1 h. The spectrum for the Al-stressed whole cells revealed peaks at 44 and 32 ppm indicative of citrate and succinate as confirmed by standards. In the control cells, the citrate was metabolized rapidly and various peaks at 94, 99, and 130 ppm were evident (Figure 2). As it appeared that succinate was being accumulated in the Al-stressed cells, the metabolism of this dicarboxylic acid was also followed in the mitochondria.

Mitochondria were isolated from Al-stressed and control cells and incubated with [2,3-^{13}C] succinate for 1 h. In the control mitochondria, succinate was

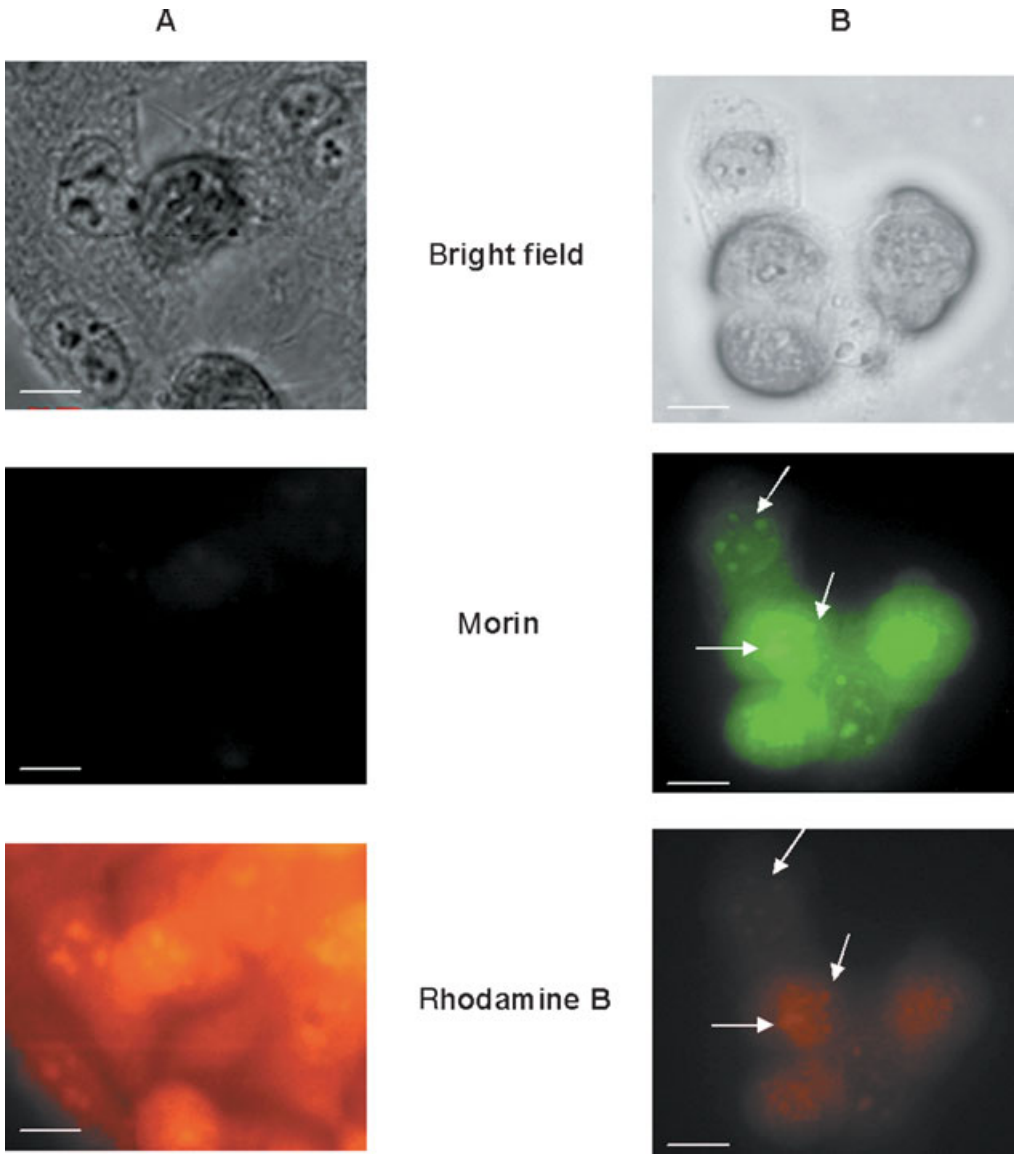

FIGURE 1. Visualization of the intracellular accumulation of Al and the mitochondrial membrane potential using morin and rhodamine B stains. HepG2 cells were grown to a minimal density on glass coverslips and exposed to (A) citrate and (B) Al–citrate for 24 h, respectively. Scale bar: 7 μm.

metabolized to an olefinic peak characteristic of fumarate (Figure 3). In the mitochondria isolated from the Al-exposed HepG2 cells, a single peak at 32–33 ppm indicative of unreacted succinate was observed, even if left for longer periods. The ability of Al to interfere with the TCA cycle was further confirmed by the presence of succinate in the spent fluid isolated from HepG2 cells exposed to Al–citrate. A peak at 12 min indicative of this dicarboxylic acid was recorded in the Al-stressed cells compared to control (Figure 4, II). Enzymatic assay involving SDH and DCPIP further confirmed this observation (Figure 4, I).

Immobilized Enzyme Assays

The disparate metabolic profile revealed by ^{13}C-NMR and HPLC studies pointed to an abnormal TCA cycle in HepG2 cells exposed to Al. To further probe the nature of this metabolic dysfunction, various key enzymes involved in the metabolism of citrate via the TCA cycle were studied by BN-PAGE, a technique known to reveal the activity and expression of enzymes. As ACN is dependent on Fe, a nutrient whose bioavailability is affected by Al, the activity and expression of this enzyme was determined. To assess the influence of Al toxicity on Fe metabolism,

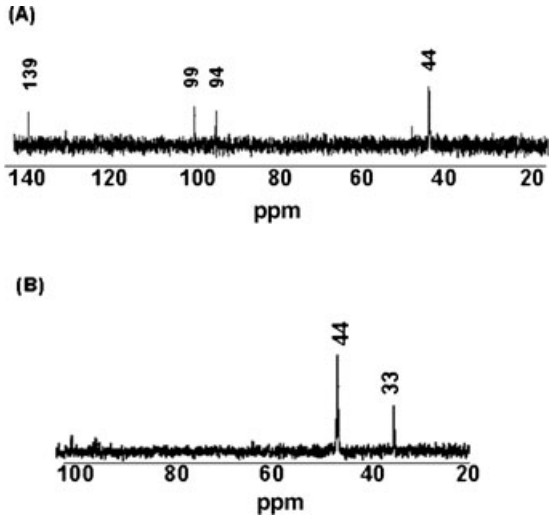

FIGURE 2. Proton-decoupled ^{13}C-NMR spectra obtained from the incubation of 10 mM [2,4-^{13}C] citrate with whole HepG2 cells from control and Al conditions. Cells were incubated for 1 h and then analyzed. (A) Citrate supplemented cultures and (B) Al–citrate supplemented cultures.

the absorption band in the 395–420 nm region that is attributed to the Fe–S cluster was monitored in the mitochondrial isolates. The mitochondria from the Al-stressed cells did not have any absorbance in the 395–420 nm region, while a prominent band was evident in the mitochondria from the control cells (Figure 5, I). In contrast, an intense absorbance shift in this region was recorded in the control cells. HepG2 mitochondria (30 μg protein equivalent) from control and Al-stressed cultures were loaded and electrophoresed.

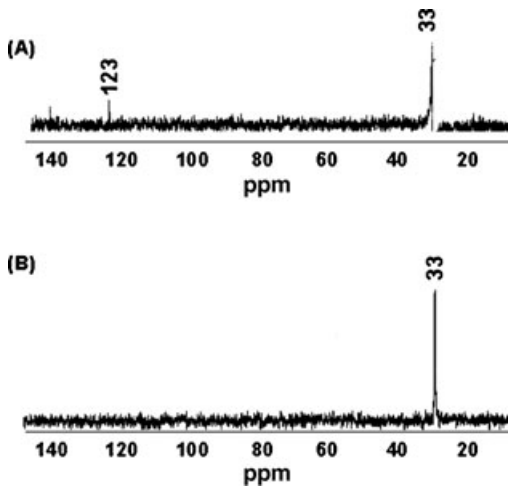

FIGURE 3. Proton-decoupled ^{13}C-NMR spectra obtained from the incubation of 5 mM [2,3-^{13}C] succinate and 1 mM NAD^+ with HepG2 mitochondria from control and Al-supplemented cultures for 1 h. Mitochondria were incubated for 1 h and then analyzed. (A) Citrate supplemented cultures and (B) Al–citrate supplemented cultures.

(I) Succinate consumption assay

Control Culture	Al-stressed Culture
0.125 ± (0.032)	1.105 ± (0.024) *

Units: μM of succinate per mL of media. S.D. in parenthesis n=3.

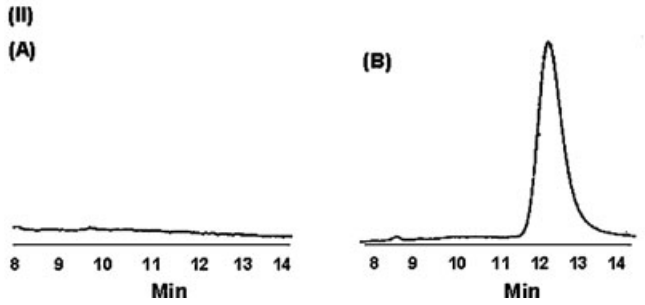

FIGURE 4. Detection of succinate in the media of control and Al-stressed cultures. (I) Succinate was measured by detecting the relative change in absorbance using the DCPIP assay. * Denotes a significant difference in comparison to control ($n = 3$, $p \leq 0.05$, mean ± SD). (II) Representative chromatographs showing the occurrence of succinate in HepG2 media from (A) citrate and (B) Al–citrate cultures. Whole cells were incubated with 10 mM citrate for 24 h at 37°C. The spent fluid was then collected and analyzed.

Both the expression and activity of the mitochondrial ACN were reduced in the HepG2 cells exposed to Al (Figure 5, II). At least a 50% decrease in activity was recorded. No activity of this citrate-isomerizing enzyme in either control or stressed cells was detected in the cytoplasm. However, Western blot experiments helped establish the presence of this protein both in the cytoplasm and mitochondria. In the latter organelle, the ACN level was markedly lower in the cells subjected to Al toxicity (Figure 5, III). In addition, the exposure of Al-stressed HepG2 cells to 5% FBS restored mitochondrial ACN levels (Figure 5, III). As these data indicated that the presence of Al affected Fe-proteins, FUM, another enzyme that relies on an Fe–S cluster for the reversible conversion of fumarate to malate was monitored. A lower activity in the HepG2 cells exposed to Al compared to the control was observed (Figure 5, IV). The inability of the Al-stressed HepG2 cells to metabolize succinate prompted us to discern the activity and expression of SDH. In-gel activity staining clearly pointed to a decrease in the activity of SDH (Figure 6, I). Coomassie staining and immunoblotting experiments revealed that this decrease in activity in the HepG2 cells subjected to Al was due to the diminution of protein expression (Figure 6, II and III).

As the mitochondria isolated from the Al-stressed cells were unable to metabolize succinate, KGDH, an enzyme involved in its formation was investigated. Incubation of control and Al-stressed mitochondria in the presence of 10 mM αKG revealed a decrease in KGDH

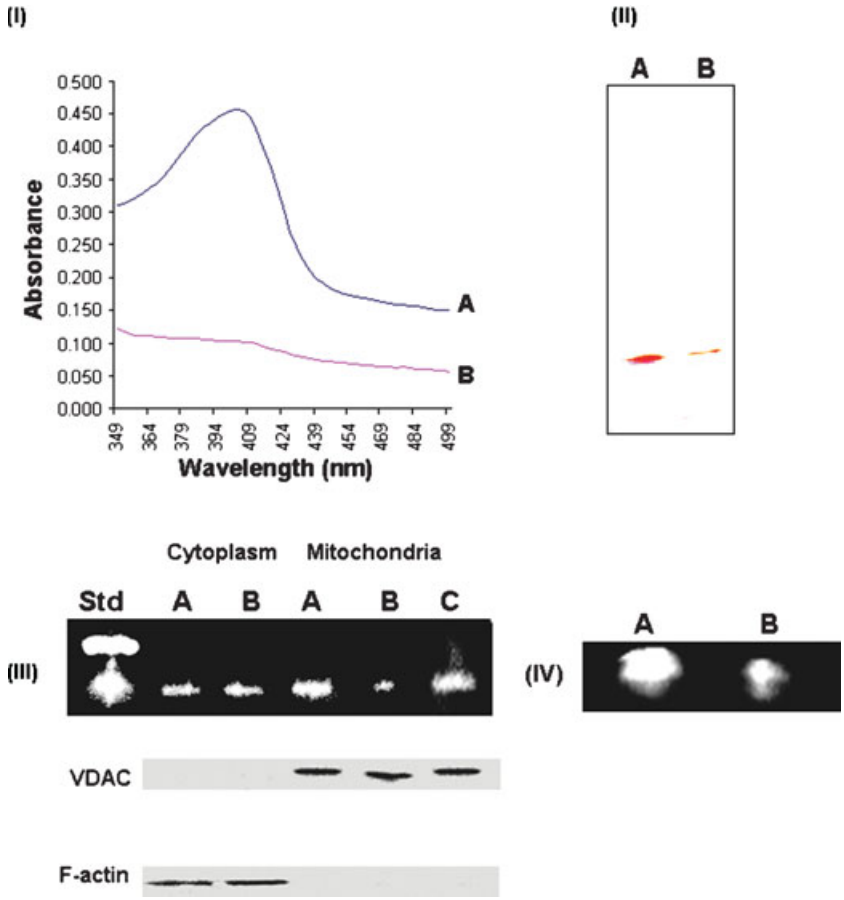

FIGURE 5. Activity and immunoblot analysis of ACN and FUM in (A) citrate (B) Al–citrate cultures, and (C) Al-stressed cells incubated in FBS for 24 h. (I) UV–VIS scan of Fe–S cluster stability in mitochondria. (II) In-gel activity stain for ACN. The border defines the respected boundaries of the gel. (III) Immunodetection of ACN in the cytoplasmic and mitochondrial fractions. Std corresponds to porcine heart ACN (Sigma). (IV) In-gel activity stain for FUM.

activity in Al-exposed HepG2 cells. While in the control experiment a fumarate peak was evident at 8 min, in the Al-stressed mitochondria a single peak at 5.5 min attributable to αKG was discerned (Figure 7, I). KGDH activity was then detected by incubation of the gel in the presence of NAD^+, CoA, and αKG. The NADH generated at the site of the enzyme formed a formazan precipitate that was easily visualized with the aid of PMS and INT. A darker band was obtained in the control sample (Figure 7, II). Densitometric analyses indicated that KGDH activity in Al-stressed cells was at least 40% lower in comparison to control. To evaluate the amount of protein associated with the change in enzymatic activity, the bands were sliced and run on a 2D BN-PAGE. Following electrophoresis, protein levels were detected by silver stain. No significant variation in protein level was discernable between control and Al-stressed cultures (Figure 7, III). This observation was further confirmed by probing these bands by SDS-PAGE and polyclonal antibodies raised against the E2-subunit of KGDH (Figure 7, IV). The intensity of the band did not appear to vary significantly in the two cases. IDH-NAD^+, an enzyme that catalyzes the decarboxylation of isocitrate to αKG, was found to be lower in activity in Al-stressed HepG2 cells as detected by formazan precipitation (Figure 8, I). On the other hand, MDH, an enzyme involved in the reversible conversion of malate to oxaloacetate, was not significantly different in the control and Al-stressed cells. Activity staining did not reveal any noticeable difference (Figure 8, II).

As numerous enzymes in the TCA cycle were markedly decreased due to the presence of Al in the medium, we decided to determine the impact of this trivalent metal on oxidative phosphorylation. Cyt C Ox, an enzyme that transfers e^- to O_2, was the obvious choice. Using diaminobenzidene as the chromophore, the activity of this protein was monitored by BN-PAGE. A dark band due to the oxidative polymerization of diaminobenzidene was observed in the mitochondrial proteins from the control cells, while no precipitation was detected in the mitochondria isolated from Al-stressed cells (Figure 9, I). These activity bands were cut

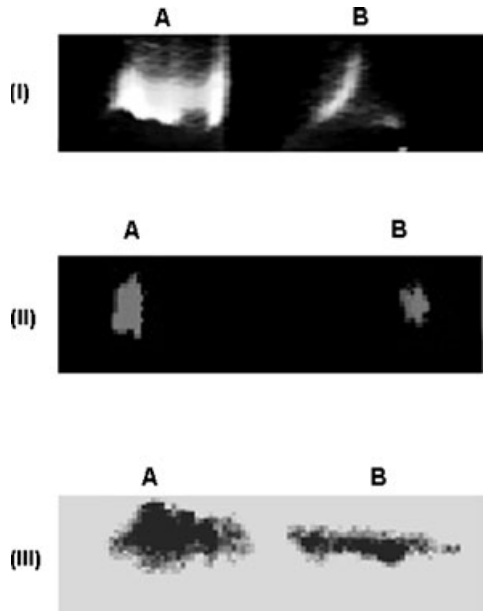

FIGURE 6. Activity and expression of SDH in (A) citrate and (B) Al–citrate cultures. (I) In-gel activity stain for SDH. (II) 2D BN-PAGE stained with Coomassie. (III) Immunodetection of SDH expression.

and further electrophoresed by the 2D BN-PAGE technique. Silver staining revealed a decreased expression of this protein in the cells exposed to Al (Figure 9, II).

DISCUSSION

These results provide evidence that points to a drastic reduction in the production of energy via oxidative phosphorylation as a consequence of Al toxicity. This is the first demonstration of the negative impact of Al on the ATP-producing machinery in oxygen-consuming cells. The ability of this trivalent metal to trigger oxidative stress and promote the accumulation of succinate is also shown. Hence, the presence of Al in a cellular environment would negatively influence the generation of ATP. Although various studies have proposed a pro-oxidant role of Al, the exact mechanism that enables Al to create an oxidative environment has not been fully understood [29]. In this study, we observed a marked increase in oxidized lipids and proteins in HepG2 cells exposed to Al. It is not unlikely that the increased levels of Al may compete for Fe-binding sites in proteins and render this Fe labile. This situation may enhance the production of reactive oxygen species (ROS), which may, in turn, lead to oxidized biomolecules. The involvement of Al in ROS production has recently been demonstrated [30]. The link between Al toxicity and a defective Fe-metabolism was further confirmed by the UV–VIS scan of mitochondrial fractions. Fe–S cluster integrity within the membrane

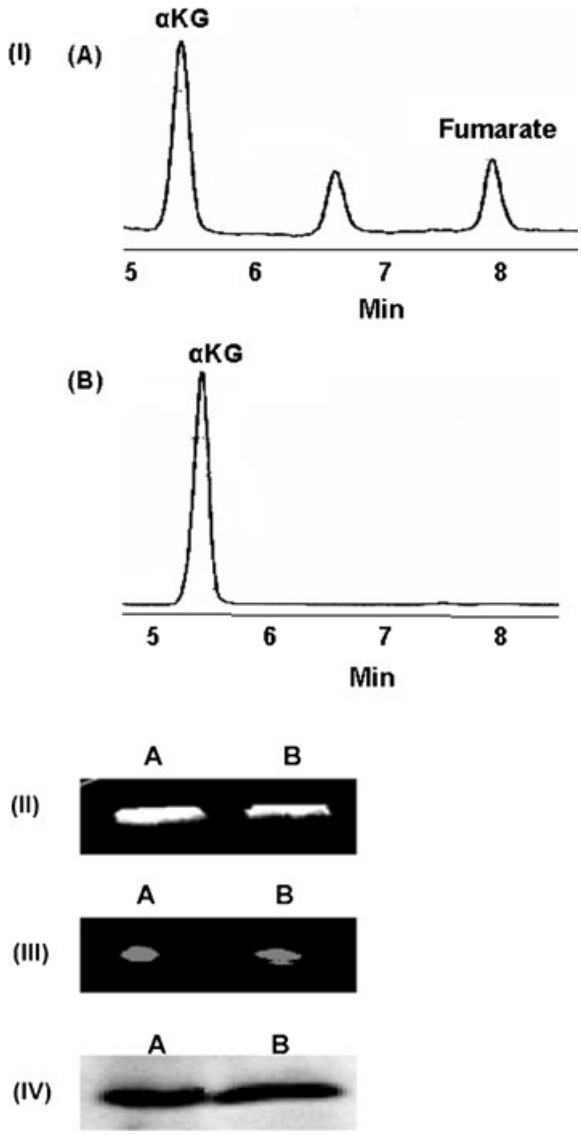

FIGURE 7. Activity and expression of KGDH in (A) citrate and (B) Al–citrate. (I) Representative chromatographs showing the consumption of 10 mM α-ketoglutarate. Mitochondria were incubated for 10 min at 37°C and then analyzed. (II) In-gel activity stain for KGDH. (III) 2D BN-PAGE stained with Coomassie R-250. (IV) Immunodetection of KGDH expression.

fraction was severely compromised in the HepG2 cells subjected to Al stress compared to the control cells. The competition between Al and Fe for binding sites in proteins is not unexpected as these two metal ions share similar charges and the concentration of Al found in this study would tilt the balance in favor of Al. The Fe–S cluster peak evident in the UV–VIS spectrum would clearly argue for such a possibility.

Thus, it is not surprising that the three critical Fe-proteins in the Al-stressed hepatocytes were severely affected as both their activity and expression were lower compared to their counterparts from the control

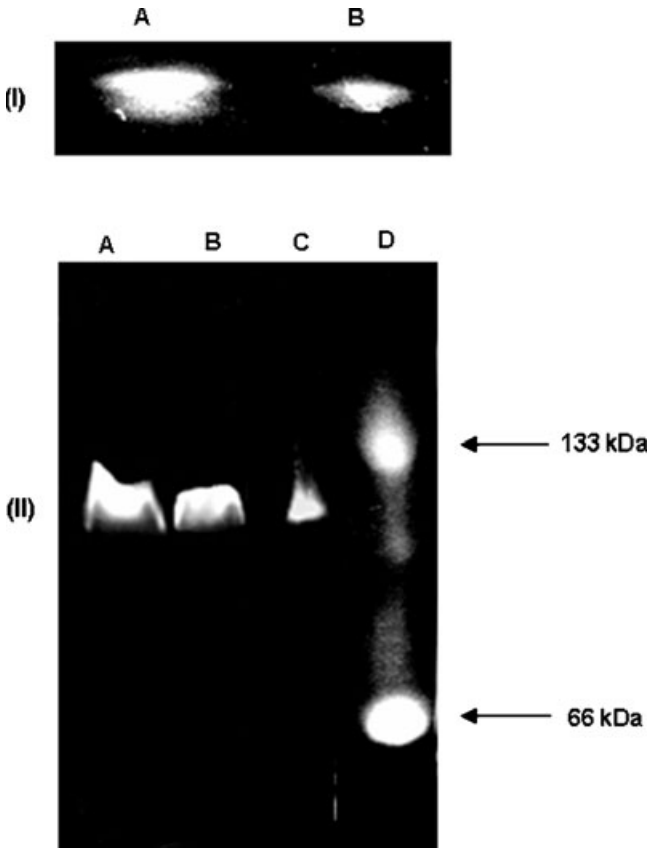

FIGURE 8. Activity staining for mitochondrial MDH and NAD^+-dependent IDH in (A) citrate, (B) Al–citrate, (C) corresponds to an MDH standard (Sigma), and (D) corresponds to a BSA standard. (I) In-gel detection of IDH-NAD^+. (II) In-gel detection of MDH.

cultures. ACN, a protein that is key to the proper functioning of the TCA cycle in the mitochondria, was markedly impeded. We have recently shown that this enzyme has lower activity in Al-stressed cells due to the perturbation of the Fe–S cluster and not its expression [8]. To promote its survival, the organism upregulates

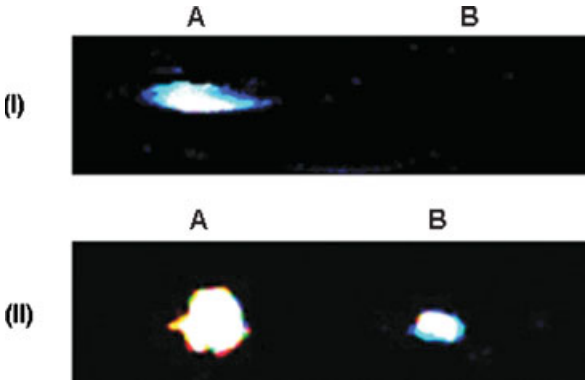

FIGURE 9. Activity staining and protein level determination for Cyt C Ox in (A) citrate and (B) Al–citrate cultures. (I) In-gel activity stain for Cyt C Ox. (II) 2D BN-PAGE detected by silver staining.

two downstream enzymes—isocitrate dehydrogenase and isocitrate lyase—in an effort to compensate for the decreased ACN activity. However, such a luxury is not affordable to these highly specialized eukaryotic cells. In this study, the HepG2 cells appeared to succumb to the toxicity of Al, as citrate was not effectively metabolized via the TCA cycle. However, the cytoplasmic ACN, a protein that acts as a sensor for oxidative stress, had negligible activity but was amply expressed in Al-stressed cells. This situation would enable this protein to monitor oxidative tension and regulate the biogenesis of Fe-proteins via the iron responsive element [31–33]. Hence, this organelle-specific control of ACN concentration may be a key strategy invoked by the HepG2 cells to survive by decreasing the TCA cycle in the mitochondria and by inhibiting the synthesis of Fe-proteins via the cytoplasmic ACN. FUM and SDH, two other Fe–S containing enzymes, were also downregulated in the Al-stressed cells. The reduction in the biosyntheses of these two enzymes would severely impede the ability of the TCA cycle to generate NADH, a crucial metabolite for the generation of ATP via oxidative phosphorylation. It is tempting to speculate that a dearth of bioavailable Fe induced by Al toxicity would create a situation whereby the formation of energy in the presence of oxygen will not be favored. The decreased syntheses of these two enzymes would certainly serve this purpose. Indeed, the Cyt C Ox, the protein that shuttles e^- directly to oxygen, was markedly diminished in the mitochondria isolated from the Al-challenged hepatocytes. Hence, it is quite likely that Al toxicity affects the production of ATP in the mitochondria by interfering with Fe-containing proteins.

The ability of the TCA cycle to be effective was further compounded by diminished activities of IDH-NAD^+ and KGDH. These two decarboxylating enzymes also play a key role in the homeostasis of NADH. This situation will undoubtedly limit the ability of the TCA cycle to generate NADH from citrate and will subsequently diminish the efficacy of the ATP-producing machinery. The slowing of the TCA cycle may have an added benefit of creating a nonoxidative environment. As the level of NADH produced is lower, the ability of the mitochondria to generate ROS when NADH is oxidized by the e^- transport proteins will also be lower. This strategy initiated in response to Al toxicity may help the cell extend its survivability due to diminished ROS formation, of course at the expense of ATP formation.

Succinate was an important metabolite that appeared to accumulate in the Al-exposed HepG2 cells. Such a situation may have been favored by the inability of the SDH and FUM from Al-stressed cells to promote the metabolism of succinate. This dicarboxylic acid has recently been proposed to play a critical role in linking

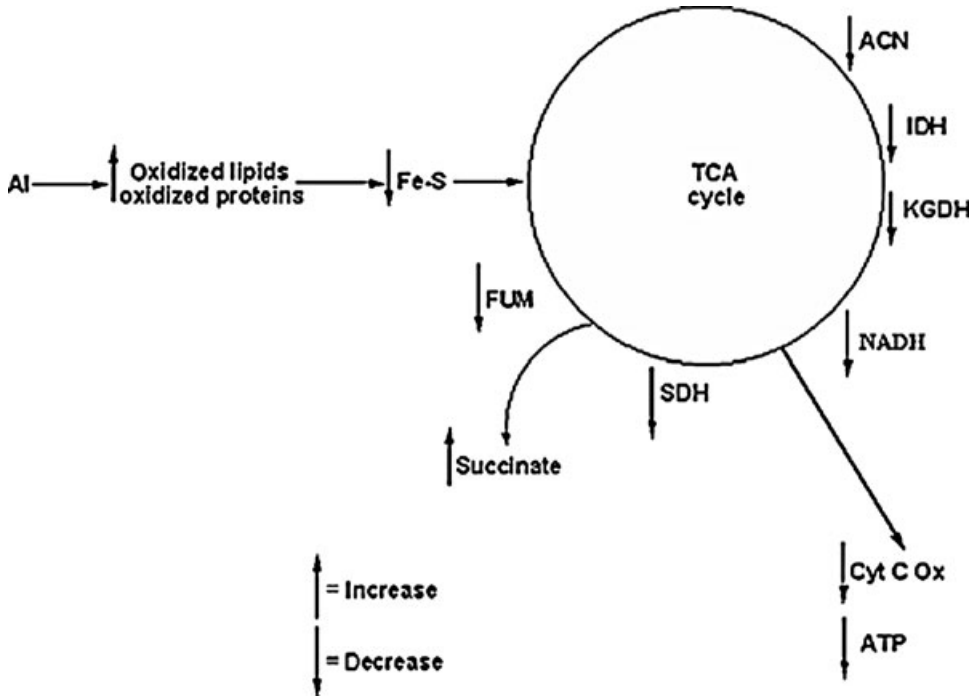

SCHEME 1. Al toxicity and mitochondrial dysfunction.

mitochondrial dysfunction to anaerobic respiration. It has been hypothesized that succinate helps stabilize HIF-1α, a subunit critical to the function of the hypoxia inducible factor (HIF). This dicarboxylic acid appears to inhibit the hydroxylation of HIF-1α and consequently prevents its degradation [34]. In the present situation, such a response to Al may not be unlikely. As this trivalent metal favors an oxidative and Fe-deprived environment, the accumulation of succinate triggered by a dysfunctional TCA cycle would be an ideal messenger, signaling the inability of mitochondria to oxidize NADH. Subsequently, the elevated level of succinate would help the cell activate its energy production via anaerobiosis with the aid of HIF-1α. The decreased activity and expression of KGDH may also contribute to the accumulation of succinate. α-Ketoacids have been widely utilized as antioxidants in vitro and their involvement in in vivo in diminishing oxidative tension has also been recently recognized [35]. The αKG may detoxify such ROS as H_2O_2 and $O_2^{-\bullet}$ with concomitant formation of succinate and CO_2. In Al-stressed HepG2 cells, the diminished activity and expression of the KGDH may serve the dual purpose of limiting the production of NADH, a pro-oxidant and decreasing oxidative tension by scavenging ROS. Hence, αKG may be an essential molecule involved in the homeostasis of ROS and succinate.

In conclusion, this work demonstrates that Al exerts its toxic influence by promoting an oxidative environment deficient in bioavailable Fe. This situation renders the TCA cycle dysfunctional and limits the production of ATP via oxidative phosphorylation. Thus, the ability of Al-stressed cells to produce ATP is severely compromised. Furthermore, the accumulation of succinate evoked by Al toxicity may be an important signaling molecule designed to shift the cellular metabolism to anaerobiosis. Scheme 1 provides a snapshot of the toxic impact of Al on TCA cycle and the oxidative energy production in hepatocytes. Thus, the negative influence of Al on the energy-generating apparatus may be an important contributing factor that enables this metal to be involved in numerous disorders.

REFERENCES

1. Kim MS, Clesceri LS. Aluminum exposure: A study of an effect on cellular growth rate. Sci Total Environ 2001;278(1–3):127–135.
2. Zatta P, Kiss T, Suwalsky M, Berthon G. Aluminum as a promoter of cellular oxidation. Coord Chem Rev 2002;228(2):271–284.
3. Nayak P. Aluminum: Impacts and disease. Environ Res 2002;89(2):101–115.
4. Singh R, Beriault R, Middaugh J, Hamel R, Chenier D, Appanna VD, Kalyuzhnyi S. Aluminum-tolerant *Pseudomonas fluorescens*: ROS toxicity and enhanced NADPH production. Extremophiles 2005;9(5):367–373.

5. Perez G, Garbossa G, Di Risio C, Vittori D, Nesse A. Disturbance of cellular iron uptake and utilisation by aluminium. J Inorg Biochem 2001;87(1–2):21–27.
6. Cairo G, Recalcati S, Pietrangelo A, Minotti G. The iron regulatory proteins: Targets and modulators of free radical reactions and oxidative damage. Free Radic Biol Med 2002;32(12):1237–1243.
7. Flora SJ, Mehta A, Satsangi K, Kannan GM, Gupta M. Aluminum-induced oxidative stress in rat brain: Response to combined administration of citric acid and HEDTA. Comp Biochem Physiol C Toxicol Pharmacol 2003;134(3):319–328.
8. Middaugh J, Hamel R, Jean-Baptiste G, Beriault R, Chenier D, Appanna VD. Aluminum triggers decreased aconitase activity via Fe–S cluster disruption and the overexpression of isocitrate dehydrogenase and isocitrate lyase: A metabolic network mediating cellular survival. J Biol Chem 2005;280(5):3159–3165.
9. Flaten TP. Aluminium as a risk factor in Alzheimer's disease, with emphasis on drinking water. Brain Res Bull 2001;55(2):187–196.
10. Naylor GJ, Sheperd B, Treliving L, McHarg A, Smith A, Ward N, Harper M. Tissue aluminum concentrations stability over time, relationship to age, and dietary intake. Biol Psychiatry 1990;27(8):884–890.
11. Smorgon C, Mari E, Atti AR, Dalla Nora E, Zamboni PF, Calzoni F, Passaro A, Fellin R. Trace elements and cognitive impairment: An elderly cohort study. Arch Gerontol Geriatr Suppl 2004;(9):393–402.
12. Berend K, van der Voet G, Boer WH. Acute aluminum encephalopathy in a dialysis center caused by a cement mortar water distribution pipe. Kidney Int 2001;59(2):746–753.
13. Harris WR, Wang Z, Hamada YZ. Competition between transferrin and the serum ligands citrate and phosphate for the binding of aluminum. Inorg Chem 2003;42(10):3262–3273.
14. Shannon JE. Tissue culture viability assays—A review of the literature. Cryobiology 1978;15(2):239–241.
15. Hsu PH. Effect of pH, phosphate and silicate on the determination of aluminum with aluminon. Soil Sci. 1963;96:230–238.
16. Johnson LV, Walsh ML, Chen LB. Localization of mitochondria in living cells with rhodamine 123. Proc Natl Acad Sci U S A 1980;77(2):990–994.
17. Uemura E, Minachi M, Lartius R. Enhanced neurite growth in cultured neuroblastoma cells exposed to aluminum. Neurosci Lett 1992;142(2):171–174.
18. Aydin S, Yargicoglu P, Derin N, Aliciguzel Y, Abidin I, Agar A. The effect of chronic restraint stress and sulfite on visual evoked potentials (VEPs): Relation to lipid peroxidation. Food Chem Toxicol 2005;43(7):1093–1101.
19. Frank J, Pompella A, Biesalski HK. Histochemical visualization of oxidant stress. Free Radic Biol Med 2000;29(11):1096–1105.
20. Kwik-Uribe CL, Reaney S, Zhu Z, Smith D. Alterations in cellular IRP-dependent iron regulation by in vitro manganese exposure in undifferentiated PC12 cells. Brain Res 2003;973(1):1–15.
21. Lee WK, Shin S, Cho SS, Park JS. Purification and characterization of glutamate dehydrogenase as another isoprotein binding to the membrane of rough endoplasmic reticulum. J Cell Biochem 1999;76(2):244–253.
22. Soum E, Brazzolotto X, Goussias C, Bouton C, Moulis JM, Mattioli TA, Drapier JC. Peroxynitrite and nitric oxide differently target the iron–sulfur cluster and amino acid residues of human iron regulatory protein 1. Biochemistry 2003;42(25):7648–7654.
23. Berndt C, Lillig CH, Wollenberg M, Bill E, Mansilla MC, de Mendoza D, Seidler A, Schwenn JD. Characterization and reconstitution of a 4Fe–4S adenylyl sulfate/phosphoadenylyl sulfate reductase from *Bacillus subtilis*. J Biol Chem 2004;279(9):7850–7855.
24. Schagger H, von Jagow G. Blue native electrophoresis for isolation of membrane protein complexes in enzymatically active form. Anal Biochem 1991;199(2):223–231.
25. Schagger H, Cramer WA, von Jagow G. Analysis of molecular masses and oligomeric states of protein complexes by blue native electrophoresis and isolation of membrane protein complexes by two-dimensional native electrophoresis. Anal Biochem 1994;217(2):220–230.
26. Seligman AM, Karnovsky MJ, Wasserkrug HL, Hanker JS. Nondroplet ultrastructural demonstration of cytochrome oxidase activity with a polymerizing osmiophilic reagent, diaminobenzidine (DAB). J Cell Biol 1968;38(1):1–14.
27. Laemmli UK. Cleavage of structural proteins during the assembly of the head of bacteriophage T4. Nature 1970;227(5259):680–685.
28. Maklashina E, Cecchini G. Comparison of catalytic activity and inhibitors of quinone reactions of succinate dehydrogenase (Succinate-ubiquinone oxidoreductase) and fumarate reductase (Menaquinol-fumarate oxidoreductase) from *Escherichia coli*. Arch Biochem Biophys 1999;369(2):223–232.
29. Exley C. The pro-oxidant activity of aluminum. Free Radic Biol Med 2004;36(3):380–387.
30. Abubakar MG, Taylor A, Ferns GA. Aluminium administration is associated with enhanced hepatic oxidant stress that may be offset by dietary vitamin E in the rat. Int J Exp Pathol 2003;84(1):49–54.
31. Campbell A. The potential role of aluminium in Alzheimer's disease. Nephrol Dial Transplant 2002;17(Suppl 2):17–20.
32. Crichton RR, Wilmet S, Legssyer R, Ward RJ. Molecular and cellular mechanisms of iron homeostasis and toxicity in mammalian cells. J Inorg Biochem 2002;91(1):9–18.
33. Ward RJ, Zhang Y, Crichton RR. Aluminium toxicity and iron homeostasis. J Inorg Biochem 2001;87(1–2):9–14.
34. Selak MA, Armour SM, MacKenzie ED, Boulahbel H, Watson DG, Mansfield KD, Pan Y, Simon MC, Thompson CB, Gottlieb E. Succinate links TCA cycle dysfunction to oncogenesis by inhibiting HIF-alpha prolyl hydroxylase. Cancer Cell 2005;7(1):77–85.
35. Varma SD, Hegde KR. Effect of alpha-ketoglutarate against selenite cataract formation. Exp Eye Res 2004;79(6):913–918.